PHYSICAL REVIEW D VOLUME 32, NUMBER 5 1 SEPTEMBER 1985

Nuclear effects in deep-inelastic lepton scattering

Edmond L. Berger
High Energy Physics Division, Argonne National Laboratory, Argonne, Illinois 60439

F. Coester
Physics Division, Argonne National Laboratory, Argonne, Illinois 60439
(Received 22 March 1985)

We present a detailed study of a conventional nuclear model in which the observed differences between the deep-inelastic structure functions of nuclei and of free nucleons, $F_2(x,Q^2)$ and $\bar{q}(x,Q^2)$, are due to scattering from exchange pions in nuclei associated with the mechanisms responsible for nuclear binding. We assume that the quark and antiquark momentum distributions of these nucleons and pions are unaffected by the nuclear medium. We write the nuclear structure functions as a sum of convolutions of (measured) isolated-hadron structure functions with hadron momentum distributions derived from nuclear potential models. We show that all but one feature of deep-inelastic neutrino and charged-lepton data are reproduced by our model. The exception is the magnitude of the excess above unity of the ratio $F_2^A(x)/F_2^D(x)$ for $x<0.2$, observed only by the European Muon Collaboration (EMC) experiment. If these EMC data are reduced in normalization by 5%, consistent with experimental uncertainties, then all features of the data are reproduced. We stress the importance of new neutrino and muon measurements at small x.

I. INTRODUCTION

Considerable interest in the particle-physics and the nuclear-physics communities was aroused initially by the observation that the inelastic structure function $F_2(x,Q^2)$ for deep-inelastic muon scattering from an iron nucleus differs significantly, as a function of the Bjorken scaling variable x, from the structure function for deuterium.[1] This phenomenon has become known as the EMC effect, based on its first observation by the European Muon Collaboration (EMC). More recent experimental work[2-5] by other groups has confirmed important features of the original data, while raising questions about the x and/or Q^2 dependences at small x ($x<0.2$). Here Q^2 is the usual square of the invariant four-momentum transfer from the initial to the final lepton.

The EMC effect has led to a wide spectrum of theoretical interpretations.[6-11] In terms of the quark-parton model, it suggests the interesting possibility that quark and antiquark degrees of freedom must be treated explicitly as degrees of freedom of the whole nucleus. Before reaching such a radical conclusion, however, one should examine in detail the conservative assumption that quarks are always confined to individual hadrons, and that nuclei are bound states described by multihadron Fock-space wave functions. Deep-inelastic lepton scattering could then be understood in terms of the quark structure of individual hadrons and the properties of the nuclear Fock-space wave functions. Such models, in which the role of quantum chromodynamics (QCD) is confined to the description of the structure of single hadrons, are natural extensions of successful nuclear theory. They are mathematically well defined, internally consistent and, most important, their predictions are sufficiently constrained so that they could be eliminated by confrontation with data. Obviously they cannot be "derived" from QCD since even bound-state wave functions of single hadrons can, at present, not be obtained in this manner.

In a previous paper[6] we examined in detail a model based on the conventional picture in which nucleons and pions are the relevant hadrons in nuclei. In this model, differences in the structure functions are due to scattering from exchange pions in nuclei associated with the mechanism responsible for nuclear binding. The internal consistency of the model depends on the use of light-front-form dynamics in which the longitudinal boosts are independent of the interactions, and particle numbers are therefore invariant under such boosts. The inclusion of other baryons, e.g., six-quark dibaryons, is a natural extension of this model. The new data, especially those obtained from experiments with ν and $\bar{\nu}$ beams, provide us with an opportunity to further test the quantitative implications of this model.

There are three main ingredients in the approach we study. First, we assume that nuclei are bound systems of nucleons and mesons. Second, we assume that the quark and antiquark momentum distributions, and thus, the deep-inelastic structure functions of these nucleons and mesons are unaffected by the nuclear medium. Third, we retain the usual assumption that nucleons contribute incoherently to the structure function of the nucleus, and we add the same incoherence assumption for the pions and other hadrons, if any. This incoherence assumption includes the assumption that final-state interactions between the residue of the struck hadron and the spectator hadrons in the nucleus do not affect the inclusive cross sections; it does not require that such final-state interactions vanish. As derived in Sec. III of Ref. 6 we can write the nuclear structure functions as a sum of convolutions of isolated-hadron structure functions with hadron momentum distri-

butions derived from nuclear Fock-space wave functions. Our prediction for the nuclear structure function per nucleon is cast in the form

$$F_2^A(x,Q^2)=\int_{z\geq x} dz\, f_N(z)F_2^N\left[\frac{x}{z},Q^2\right] + \int_{y\geq x} dy\, f_\pi(y)F_2^\pi\left[\frac{x}{y},Q^2\right] + \int_{z\geq x} dz\, f_B(z)F_2^B\left[\frac{x}{z},Q^2\right]. \quad (1.1)$$

In Eq. (1.1), $F_2^N(x,Q^2)$ and $F_2^\pi(x,Q^2)$ are structure functions measured on unbound nucleons and mesons, respectively, and $F_2^B(x,Q^2)$ is the structure function of some other baryon with baryon number n_B [e.g., a $\Delta(1236)$ or a six-quark dibaryon]. In Ref. 6, we used specific nuclear potential models to derive expressions for the magnitudes and momentum dependences of $f_\pi(y)$ and $f_N(z)$ which represent the densities of mesons and nucleons carrying (light-front) fractional longitudinal momenta y and z. The momentum distributions per nucleon, $f_N(z)$, $f_B(z)$ and $f_\pi(y)$, must, by definition, satisfy the relations

$$\int dz\, f_N(z)+n_B\int dz\, f_B(z)=1 \quad (1.2)$$

(baryon-number conservation) and

$$\int dz\, z f_N(z)+\int dy\, y f_\pi(y)+\int dz\, z f_B(z)=1 \quad (1.3)$$

(momentum conservation). We emphasize that the momentum-balance relation (1.3) is inescapable in our model; in each Fock-space amplitude of a bound state the sum of the light-front momentum fractions of all constituent particles is constrained to a constant value, which we choose to be A.

Other pion models[7] focus on a medium-dependent enhancement of the pion clouds of individual nucleons. They arrive at a convolution formula for the pionic enhancement of the structure function,

$$\delta_\pi F_2^A(x,Q^2)=\int_{y\geq x} dy\, f_\pi(y)F_2^\pi\left[\frac{x}{y},Q^2\right], \quad (1.4)$$

without the necessity for the constraint (1.3). In these models the function $f_\pi(y)$ is not related to a nuclear wave function in a manner which defines it *a priori* as a probability density of excess pions. It is so interpreted *a posteriori* because of its appearance in the convolution formula.

In this paper, the integral $\langle n_\pi\rangle=\int f_\pi(y)dy$ is the mean number of excess pions per nucleon associated with the pion exchanges in the nucleus, and $\langle y\rangle\equiv\int y f_\pi(y)dy$ is the fraction per nucleon of the momentum of the nucleus carried by the exchange pions. Our quantitative results are insensitive to the precise functional shape of $f_\pi(y)$, and are controlled mainly by $\langle n_\pi\rangle$ and $\langle y\rangle$.

In Sec. II of this paper we establish our notation, and we summarize the data available, discuss their consistency, and offer some qualitative observations on their implications. Throughout this paper we use $R_{\rm EMC}$ to denote the ratio $F_2^A(x,Q^2)/F_2^{\rm D}(x,Q^2)$. The subscript EMC is helpful, if not indeed necessary, to avoid confusion with the traditional use of R to denote the ratio of the cross sections for absorption of longitudinal and transverse currents, σ_L/σ_T.

In Sec. III, we discuss our exchange pion model in some detail, emphasizing in a relatively model-independent manner its implications for the valence and sea-quark momentum distributions of nucleons in nuclei. Subsequently, we describe how we obtain the nucleon and pion momentum distributions $f_N(z)$ and $f_\pi(y)$ in a nucleus from nuclear potential models, and we present the free nucleon and meson structure functions we employ.

We present our comparisons with data in Sec. IV. This section includes a description of the nuclear A dependence of $F_2^A(x,Q^2)$ which we expect. The new information from neutrino experiments is expressed best in terms of a potential enhancement of the antiquark content $\bar{q}^A(x)$ of nucleons embedded in nuclei. We show that the predictions of our model for $\bar{q}^A(x)$ are in agreement with the data. Finally, in Sec. IV, we comment on alternative approaches to interpreting the EMC effect and contrast our predictions with some of theirs.

Our conclusions, summarized in Sec. V, are that all but one important feature of the data are reproduced by the conventional nuclear model which we study. The exception is the magnitude of the excess above unity of the ratio $R_{\rm EMC}(x)=F_2^A(x)/F_2^{\rm D}(x)$ for $x<0.2$, observed only by the original EMC experiment.[1] Our approach reproduces the magnitude and shape of the depression of $R_{\rm EMC}(x)$ below unity for $0.2<x<0.6$, observed by all experiments, the rise of $R_{\rm EMC}(x)$ above unity as $x\to 1$, and the weak enhancement of $\bar{q}^A(x)$ demonstrated by the neutrino experiments. If the normalization of the EMC data on $R_{\rm EMC}(x,Q^2)$ is reduced by 5%, our conventional model would be in perfect agreement. This 5% reduction is within the range of experimental normalization uncertainties.[1] On the other hand, if the magnitude of the low-x enhancement in $R_{\rm EMC}$ is confirmed, then, as we argued in Ref. 6, its explanation requires a modification of one or more of our three basic assumptions. In a picture in which a free nucleon is represented as a core surrounded by a cloud of mesons, it seems quite plausible that the properties of the cloud would be modified when the nucleon is embedded in a nucleus. This would imply that $F_2^N(x,Q^2)$ is altered, in contrast to our assumption. We find that an *ad hoc* increase of the nucleon ocean in iron by about 10% could reproduce the low-x enhancement of the EMC ratio without violating any other data. This increase can be interpreted as an increase of the pion cloud of individual nucleons. Alternatively, the same effect could be achieved by a modest alteration of the valence structure without *ad hoc* increase of the ocean. Such an alteration of the valence quark distribution could not easily be blamed on the pion cloud and may be indicative of a large core size, or the presence of other baryon states in the nucleus. Because the low-x enhancement in $R_{\rm EMC}(x,Q^2)$ is observed only for $Q^2\gtrsim 10$ GeV^2, it is possible that there is a threshold in Q^2 associated with the A-dependent alteration of $F_2^N(x,Q^2)$. From the point of view of demonstrating clearly that the nuclear medium af-

fects the parton degrees of freedom in an essential way, it is clearly crucial to carry out a careful series of experiments focused on the Q^2 and A dependences of $F_2^A(x,Q^2)$ at small x ($0<x<0.2$).

II. SURVEY OF PERTINENT DATA; NOTATION

A. Deep-inelastic muon and electron scattering

The measured doubly differential cross section $d^2\sigma/dQ^2dx$ may be expressed in terms of the inelastic structure function per nucleon, $F_2(x,Q^2)$, as

$$\frac{d^2\sigma}{dQ^2dx}=\frac{4\pi\alpha^2}{Q^4x}\left[(1-y)+\frac{y^2}{2(1+R)}\right]F_2(x,Q^2)\ . \tag{2.1}$$

In Eq. (2.1), $y=Q^2/2MEx$, where E is the laboratory energy of the incident lepton, and $R=\sigma_L/\sigma_T$ is the ratio of the cross sections for absorption of longitudinally and transversely polarized virtual photons.

In Fig. 1, we collect available data[1-3] on the ratio of the differential cross sections for the scattering from iron (Fe) and from deuterium (D):

$$\frac{\sigma^{\rm Fe}(x,Q^2)}{\sigma^{\rm D}(x,Q^2)}\ . \tag{2.2}$$

Our calculation, carried out in the context of the quark parton model, yields predictions for $F_2^A(x,Q^2)$ and, therefore, we wish to interpret the data in Fig. 1 as the ratio of the structure functions, $F_2^{\rm Fe}(x,Q^2)/F_2^{\rm D}(x,Q^2)$. Inspection of Eq. (2.1) shows that this ratio is precisely equal to the ratio of the cross sections, if $R=\sigma_L/\sigma_T$ is independent of the baryon number A of the nucleus.

In the cases of the EMC and BCDMS data, R is measured to be negligible for the ranges of x and Q^2 represented in Fig. 1. Correspondingly, for these two experiments, the data points represent the ratio $F_2^{\rm Fe}/F_2^{\rm D}$ unambiguously. In the case of the SLAC data, the measured values of σ_L/σ_T are not negligible and *may* exhibit dependence on A. Unfortunately, the SLAC measurements of R have been made thus far only in the region of x where no discrepancy is observed in Fig. 1 between the SLAC eN and the CERN μN data samples. For $Q^2=5$ GeV^2, and an *average* $x=0.5$, the measurements provide $R_{\rm Fe}-R_{\rm D}=0.152\pm0.066$, a two-standard-deviation effect. It has been noticed by several authors[12] that if one assumes that this average value applies for all x, then one can extract from the SLAC data an experimental ratio $F_2^{\rm Fe}(x,Q^2)/F_2^{\rm D}(x,Q^2)$ which agrees well with the CERN μN data, *including* the magnitude of the excess of $R_{\rm EMC}$ above unity for $x<0.2$. Given the uncertainties in the data themselves and in the assumption of x independence, we prefer to leave the data unaltered. Throughout this paper we will use data on the ratio $R_{\rm EMC}(x,Q^2)$ defined in Eq. (2.2) and as published by the experimenters. Our theoretical curves, however, will always be the ratio $F_2^A(x,Q^2)/F_2^{\rm D}(x,Q^2)$.

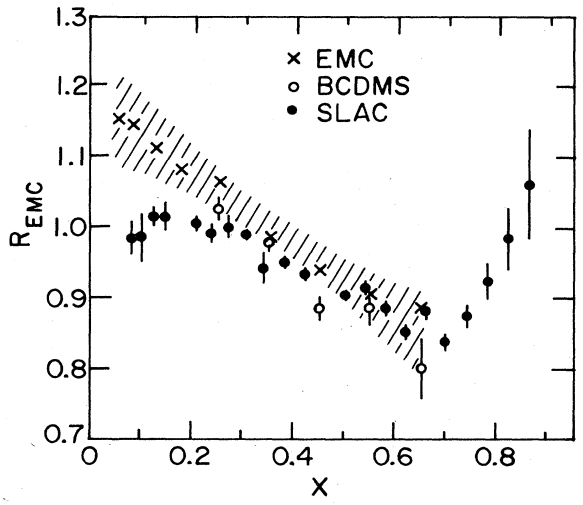

FIG. 1. Compilation of data on the ratio of structure functions $F_2^{\rm Fe}(x,Q^2)/F_2^{\rm D}(x,Q^2)$ for deep-inelastic electron and muon scattering, plotted as a function of x. Shown are published results from the EMC Collaboration (Ref. 1), from the BCDMS collaboration (Ref. 3), and from SLAC experiments (Ref. 2).

In addition to the influences of σ_L/σ_T, other phenomena may contribute to the different patterns exhibited at low x in Fig. 1. These include possible dependence of $R_{\rm EMC}(x,Q^2)$ on Q^2, and a possible error of up to 7% in the relative normalization of the iron and deuterium data.[1] The shaded band in Fig. 1 indicates the EMC group's estimate of experimental systematic uncertainties. The EMC and BCDMS data samples were obtained at large Q^2 (EMC: $\langle Q^2\rangle\simeq 200x$ GeV^2), whereas the SLAC data points at low x are associated with Q^2 of 2 and 5 GeV^2. While only a small dependence of $R_{\rm EMC}$ on Q^2 ($\simeq 10\%$ between $Q^2=5$ and 20 GeV^2) is needed at small x to bring the SLAC and CERN data into agreement, there is no evidence within the individual data samples for a trend of this sort.

Among the qualitative features evident in Fig. 1, all experiments agree upon the depression of $R_{\rm EMC}$ below unity in the region $0.2<x<0.8$. Only the SLAC data extend coverage to x large enough to observe an increase of $R_{\rm EMC}$ with x as $x\to 1$. For $x<0.2$, the CERN EMC data show a pronounced rise of $R_{\rm EMC}(x,Q^2)$ as $x\to 0$, whereas the SLAC data indicate no enhancement of $R_{\rm EMC}$ above unity in this region of x. Since Fe and D each contain approximately equal numbers of neutrons and protons, and thus, equal numbers of up and down quarks, the effects shown in Fig. 1 are not associated with a difference in the x dependences of up- and down-quark densities $u(x)$ and $d(x)$. Traditional interpretations of the quark-parton model led to the expectation that $R_{\rm EMC}(x)$ would be very nearly unity an show no significant dependence on x for $x\gtrsim 0.05$.

B. Structure functions in the parton model

For deep-inelastic muon or electron scattering, $F_2(x,Q^2)$ may be expressed as a sum over contributions from the different quark and antiquark flavors:

$$F_2(x,Q^2)=x\sum_f e_f^2[q_f(x,Q^2)+\bar{q}_f(x,Q^2)]\ . \tag{2.3}$$

Here e_f denotes the fractional charge of the quark of flavor f, and q_f ($\bar{q}_f$) are the quark (antiquark) probability

distributions. For deep-inelastic neutrino scattering, Eq. (2.3) is replaced by one in which the factor e_f^2 is omitted.

An isoscalar nucleus N contains equal numbers of protons and neutrons. Thus,

$$F_2^N(x,Q^2)\equiv\tfrac{1}{2}[F_2^p(x,Q^2)+F_2^n(x,Q^2)]\ , \tag{2.4}$$

where F_2^p and F_2^n are the structure functions of free protons and neutrons, respectively. Isospin symmetry relationships between up- and down-quark densities in the proton and neutron state that $u^p(x)=d^n(x)$, $d^p(x)=u^n(x)$. Likewise, for the strange-quark content, $s^p(x)=s^n(x)$. For deep-inelastic muon and electron scattering these allow us to rewrite Eq. (2.4) as

$$F_2^{\mu N}(x,Q^2)=\tfrac{1}{2}\{\tfrac{5}{9}x[u(x)+\bar{u}(x)+d(x)+\bar{d}(x)] +\tfrac{4}{9}xs(x)\}\ . \tag{2.5}$$

In Eq. (2.5), all quark and antiquark densities refer to those for *free protons*; $s(x)=\bar{s}(x)$ is assumed, and we ignore any contributions from the charm sea. The Q^2 dependence of the densities on the right-hand side has been suppressed in the notation.

Making the usual decomposition of $u(x)$ and $d(x)$ into valence and sea components, $u_{\rm val}(x)=u(x)-\bar{u}(x)$, we may define the valence and sea components of an isoscalar nucleon as

$$V^N(x)=\tfrac{1}{2}[u_{\rm val}(x)+d_{\rm val}(x)]\ , \tag{2.6}$$

$$S^N(x)=\tfrac{1}{2}[\bar{u}(x)+\bar{d}(x)]\ . \tag{2.7}$$

Because the total number of valence quarks in a proton is three, we have $\int V_N(x)dx=\frac{3}{2}$.

In terms of Eqs. (2.5)–(2.7), we obtain

$$F_2^{\mu N}(x,Q^2)=x[\tfrac{5}{9}V^N(x,Q^2)+\tfrac{10}{9}S^N(x,Q^2)+\tfrac{2}{9}s(x,Q^2)]\ . \tag{2.8}$$

The further assumption of SU(3) symmetry for the ocean would allow us to simplify Eq. (2.8) by equating $s(x)$ with $S^N(x)$.

The rise of $R_{\rm EMC}$ with x as $x\to1$ is usually interpreted in terms of Fermi smearing. In the region $0.2<x<0.8$, the valence quarks dominate the behavior of $F_2(x,Q^2)$. Correspondingly, the depression of $R_{\rm EMC}$ below unity in this region of x indicates a decrease with A of the valence-quark momentum distribution for $x>0.2$, i.e., a degradation of momentum carried by the valence quarks. For $x<0.2$, both valence and sea quarks contribute significantly to $F_2(x,Q^2)$, with the sea becoming increasingly important as $x\to0$. The rise of $R_{\rm EMC}(x,Q^2)$ as $x\to0$ has been discussed in terms of a significant increase of the sea[8] with A, an interpretation challenged by neutrino data, as discussed below.

C. Neutrino and antineutrino experiments

The doubly differential cross sections for deep-inelastic neutrino and antineutrino scattering are

$$\frac{d^2\sigma^{(\nu,\bar{\nu})}}{dx\,dy}=\frac{G^2ME}{\pi}\left\{\left[(1-y)+\frac{y^2}{2(R+1)}\right]F_2^{(\nu,\bar{\nu})}(x,Q^2) \pm\left[y-\frac{y^2}{2}\right]xF_3^{(\nu,\bar{\nu})}(x,Q^2)\right\}\ . \tag{2.9}$$

Here $R=\sigma_L/\sigma_T=F_L/2xF_1$, with $F_L=F_2-2xF_1$.

Again, if isospin invariance is assumed and the contributions of heavy flavors such as charm are neglected, the structure functions per nucleon for scattering from an isoscalar target N may be expressed as

$$2xF_1^{\nu N}=2xF_1^{\bar{\nu}N}=x(u+d+\bar{u}+\bar{d}+2s)\ , \tag{2.10}$$

$$xF_3^{\nu N}=x(u+d-\bar{u}-\bar{d}+2s)\ , \tag{2.11a}$$

$$xF_3^{\bar{\nu}N}=x(u+d-\bar{u}-\bar{d}-2s)\ . \tag{2.11b}$$

In the simple case in which $R=0$, $F_2=2xF_1$, and Eq. (2.9) may be rewritten as

$$\frac{d^2\sigma^{\nu N}}{dx\,dy}=\frac{G^2ME}{\pi}x[(u+d+2s)+(1-y)^2(\bar{u}+\bar{d})]\ , \tag{2.12a}$$

$$\frac{d^2\sigma^{\bar{\nu}N}}{dx\,dy}=\frac{G^2ME}{\pi}x[(\bar{u}+\bar{d}+2\bar{s})+(1-y)^2(u+d)]\ . \tag{2.12b}$$

Inspection of Eq. (2.12) shows that one may extract the separate momentum distributions of the quark and antiquark contributions either from data on the y distributions at large y or from linear combinations of $\sigma^{\nu N}$ and $\sigma^{\bar{\nu}N}$. Particularly interesting for the purposes of this paper are the *antiquark* momentum distribution

$$x\bar{q}(x,Q^2)\equiv x(\bar{u}+\bar{d}+2\bar{s})\ , \tag{2.13}$$

obtained from $\sigma^{\bar{\nu}N}(x,y)$ at large y, and the *valence*-quark momentum distribution

$$xV^N(x)=\tfrac{1}{2}x(u+d-\bar{u}-\bar{d})\ , \tag{2.14}$$

obtained from the difference $\sigma^{\nu N}-\sigma^{\bar{\nu}N}$. [$V^N(x)$ was defined previously in Eq. (2.6).] Our calculations of the nuclear A dependence of these quantities are described in Sec. III. In the remaining paragraphs of this section we summarize the available neutrino data.

In the CDHS experiment,[4] the sea combination $x(\bar{u}+\bar{d}+2\bar{s})$ observed in Fe is extracted from the antineutrino y distribution at large y, and the $x(\bar{d}+\bar{s})$ sea observed in hydrogen is also extracted in a similar fashion. Their ratio is reproduced here as $R_{\bar{q}}$ in Fig. 2. No significant deviation from unity is observed. For the ratio of the seas integrated over x,

$$K_{\bar{q}}\equiv\frac{\int dx\,x(\bar{u}+\bar{d}+2\bar{s})^{\rm Fe}}{2\int dx\,x(\bar{d}+\bar{s})^p}\ , \tag{2.15}$$

a value of $1.10\pm0.11\pm0.07$ is quoted.[4] These data correspond to an average $Q^2\simeq66x$. The ratio $F_2^{\rm Fe}(x)/F_2^p(x)$ is also studied in the CDHS neutrino experiment. While no significant deviation from unity is observed,[4] the results also agree within experimental uncertainties with the

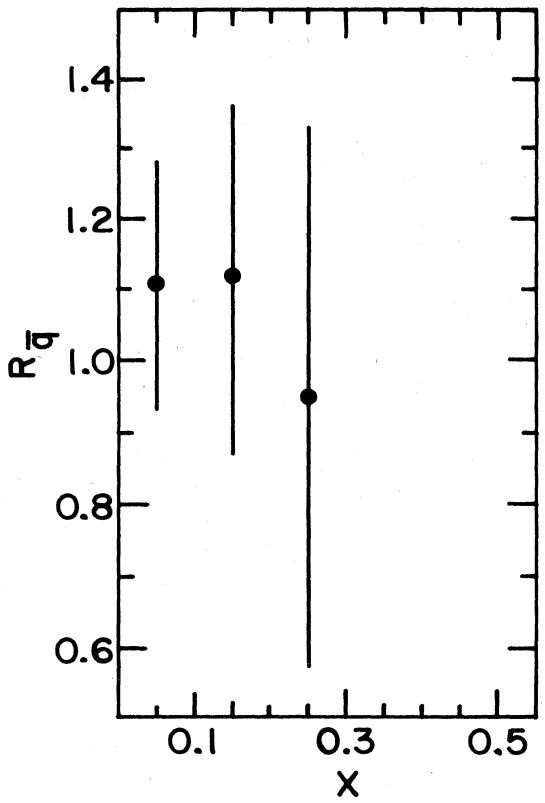

FIG. 2. The ratio $R_{\bar{q}}(x)$ is plotted versus x. Here $R_{\bar{q}}$ is defined as the ocean combination $x(\bar{u}+\bar{d}+2\bar{s})$ observed in Fe divided by twice the combination $x(\bar{d}+\bar{s})$ observed in hydrogen. The data are from the CDHS collaboration (Ref. 4).

SLAC results on $F_2^{eFe}(x)/F_2^{eD}(x)$. The neutrino data[4] on $R_{EMC}(x)$ disagree with the rise at small x observed in Ref. 1. As remarked above in our discussion of the comparison of the EMC and SLAC data, it is possible that the discrepancy at small x may be due to the fact that the neutrino results are obtained at smaller values of Q^2.

A comparison of ν and $\bar{\nu}$ data on H_2 and Ne was made by the BEBC TST group, and one of $\bar{\nu}$ data on D_2 and Ne was made by the BEBC WA25/WA59 group.[5] The ratios of the cross sections $d^2\sigma/dy\,dx$ show no rise at small x or at large y. According to the analysis of Sarkar-Cooper *et al.*,[5] a large (e.g., 35%) increase in the sea distribution can be excluded, whereas some support is found for a softening of the valence-quark momentum distribution. At low x, the Q^2 range spanned by these $\nu,\bar{\nu}$ data is $2<Q^2<10$ GeV^2, with $\langle Q^2\rangle=3.7$ GeV^2 at $x=0.075$, but no Q^2 variation is observed across the entire x,y plane.[5] The $\bar{\nu}$Ne, $\bar{\nu}D_2$ data also do not support A dependence of $R=\sigma_L/\sigma_T$ as a possible explanation for the discrepancy at small x between the original EMC data on R_{EMC} and all other data.

D. Massive-lepton-pair production

Neutrino data provide the most direct way to extract the antiquark distribution functions of nucleons. Massive-lepton-pair production—the Drell-Yan process—offers another method. As has been discussed by several authors,[13] the A dependence of the cross section $\sigma(pN\to\gamma^*X)$ in carefully chosen kinematic regions is determined by the A dependence of the ocean quark distributions of the target N. To the accuracy of the data available, no significant dependence on A is observed.[14]

III. PION-EXCHANGE MODEL

We assume that a nucleus consists of nucleons and pions, the pions being identified with the meson exchange forces responsible for nuclear binding. We implicitly ignore both the pionic self-energy and the pions in the meson cloud of isolated nucleons, and thus we deal only with pions associated with pion exchange. We assume that the unitary representations of the Poincaré transformations are of the "front form."[15] In this form longitudinal boosts are independent of the interactions and the pion numbers are therefore invariant under such boosts. We define a light-front momentum fraction per nucleon,

$$y=\frac{Ap_+^{\pi}}{p_+^{A}} \tag{3.1}$$

for pions, and a similar quantity for nucleons,

$$z=\frac{Ap_+^{N}}{p_+^{A}}\ , \tag{3.2}$$

where the $+$ component of any four-vector is defined as the sum of the longitudinal component and the time component. The quantity A is the number of nucleons, and the superscript A is used to denote the entire nucleus. The fractions y and z are invariant under longitudinal Lorentz boosts. Functions $f_N(z)$ and $f_\pi(y)$ are defined as functionals of the Fock-space amplitudes such that they specify, respectively, the number density of nucleons and the number density of exchange pions. The mean number of exchange pions per nucleon is

$$\langle n_\pi\rangle=\int f_\pi(y)dy\ , \tag{3.3}$$

and the mean momentum (per nucleon) carried by these pions is

$$\langle y\rangle=\int yf_\pi(y)dy\ . \tag{3.4}$$

The mean number of nucleons, per nucleon, is obviously unity. Thus, the function $f_N(z)$ satisfies the normalization integral

$$\int f_N(z)dz=1\ . \tag{3.5}$$

In our approach $f_\pi(y)$ and $f_N(z)$ are derived explicitly from a unified framework in which conservation of momentum holds. It requires that

$$\int yf_\pi(y)dy+\int zf_N(z)dz=1\ . \tag{3.6}$$

The variables y and z range over the interval 0 to A, but, in practice, $f_\pi(y)$ has its main support for $y<1$, and $f_N(z)$ has its main support in the neighborhood of $z=1$.

As indicated in the Introduction the internal consistency of our approach depends on the use of light-front-form dynamics, in which the hadrons are "on mass shell," "on p^+ shell," and "off p^- shell," where $p^{\pm}=p^3\pm p^0$. Con-

fusion can easily be created by arguments based on either instant form dynamics, where the three-momentum is trivially conserved and the particles are "off energy shell," or a covariant Green's function formalism, where the four-momentum is trivially conserved and the particles are "off mass shell."

In terms of the picture presented here, the structure function $F_2^A(x)$ extracted from data obtained on a nuclear target receives contributions from two sources. The deep-inelastic virtual gauge boson interacts with the constituents of either a pion or a nucleon in the nucleus. Equation (1.1) was derived in Ref. 6 for large Q^2 under the assumptions that the nucleus is a bound system of A nucleons and an indefinite number of pions, and that the nucleons and pions contribute incoherently to the structure function of the nucleus.

By following a derivation entirely analogous to that which led to Eq. (1.1), we also may derive statements for the nuclear quark and antiquark number densities, per nucleon. These are

$$q^A(x,Q^2)=\int_{y\geq x}\frac{dy}{y}f_\pi(y)q^\pi\left[\frac{x}{y},Q^2\right]+\int_{z\geq x}\frac{dz}{z}f_N(z)q^N\left[\frac{x}{z},Q^2\right] \tag{3.7}$$

and

$$\bar{q}^A(x,Q^2)=\int_{y\geq x}\frac{dy}{y}f_\pi(y)\bar{q}^\pi\left[\frac{x}{y},Q^2\right]+\int_{z\geq x}\frac{dz}{z}f_N(z)\bar{q}^N\left[\frac{x}{z},Q^2\right]. \tag{3.8}$$

Equations (3.7) and (3.8) apply for each quark flavor (i.e., $q=u,d,\ldots$).

Because pions contain *valence* antiquarks, Eq. (3.8) implies a potentially dramatic difference between the antiquark distributions of free and bound nucleons. Unfortunately, as shown in the results described in Sec. IV, these differences do not become significant until $x\gtrsim 0.3$ where data are sparse.

The valence-quark distribution is obtained as the difference

$$q_{\rm val}^A(x)=q^A(x)-\bar{q}^A(x)\ .$$

For "isoscalar pions," appropriate in our context, $q^\pi(x)\equiv\bar{q}^\pi(x)$. Thus, from Eqs. (3.7) and (3.8) we derive

$$q_{\rm val}^A(x,Q^2)=\int_{z\geq x}\frac{dz}{z}f_N(z)q_{\rm val}^N\left[\frac{x}{z},Q^2\right]. \tag{3.9}$$

One sees clearly from Eq. (3.9) that the pion contribution $f_\pi(y)$ does not affect the valence-quark distribution function.

Several quantitative and qualitative conclusions may be drawn directly from Eqs. (3.7)—(3.9) which are entirely independent of the numerical details of our computation. These include the following.

(i) Because $\int f_N(z)dz=1$, we preserve the number of valence quarks per nucleon:

$$\int q_{\rm val}^A(x)dx=\int q_{\rm val}^N(x)dx\ . \tag{3.10}$$

(ii) The net momentum carried by valence quarks is reduced:

$$\int xq_{\rm val}^A(x)dx=\langle z\rangle\int xq_{\rm val}^N(x)dx\ . \tag{3.11}$$

According to Eq. (3.6), $\langle z\rangle=1-\langle y\rangle$ in our approach. Given our parameters, as discussed in Sec. IV, this is roughly a 5% reduction. The shape of the nucleon distribution, $f_N(z)$, has only a modest dependence on A. The more significant A dependence of $q_{\rm val}^A(x)$ is due to the A dependence of $\langle y\rangle$ which is determined by the density of pions. Our success in describing the data on $R_{\rm EMC}(x)$ for $0.3<x<0.8$ is determined by $\langle y\rangle$.

(iii) Because $f_N(z)$ has its main support in the neighborhood of $z=1$, Eq. (3.9) shows that there will be little difference between $q_{\rm val}^A(x)$ and $q_{\rm val}^A(x)$ at small x.

(iv) The relative simplicity of Eq. (3.9) suggests strongly that experimental results on the A dependence of $q_{\rm val}^A(x,Q^2)$ would be very useful. Such information has not yet been extracted from the neutrino data.

(v) In deep-inelastic neutrino scattering, the integral $\int F_2^{\nu N}(x)dx$ represents the total momentum fraction carried by quark and antiquark constituents in the nucleon. We note that this integral is not necessarily left invariant. Employing Eqs. (1.1) and (3.6) one may show that

$$\int F_2^A(x)dx-\int F_2^N(x)dx=\langle y\rangle\left[\int F_2^\pi(x)dx-\int F_2^N(x)dx\right]. \tag{3.12}$$

Thus,

$$\int F_2^A(x)dx=\int F_2^N(x)dx$$

only if $\langle y\rangle=0$ or if

$$\int F_2^\pi(x)dx=\int F_2^N(x)dx\ .$$

Moreover, we see that the fractional increase in the momentum fraction carried by the quarks and antiquarks is

$$\langle y\rangle\left[\frac{\int F_2^\pi(x)dx}{\int F_2^N(x)dx}-1\right]. \tag{3.13}$$

In our explicit calculations, $\langle y\rangle$ is of order 0.05. Correspondingly, the exchange pions do not lead to a significant change in the net momentum fraction carried by quarks and antiquarks.

(vi) Employing Eqs. (3.7) and (3.9), we derive

$$\int x\bar{q}^A(x)dx-\int x\bar{q}^N(x)dx=\langle y\rangle\left[\int x\bar{q}^\pi(x)dx-\int x\bar{q}^N(x)dx\right]. \tag{3.14}$$

For the specific structure functions discussed below in Sec. III B, $\int x\bar{q}^N(x)dx=0.05$ for the sum $\bar{u}+\bar{d}$, whereas $\int x\bar{q}^\pi(x)dx=0.23$. Thus, Eq. (3.14) implies that the fractional momentum per nucleon carried by $\bar{u}$ and $\bar{d}$ antiquarks increases by $0.18\langle y\rangle\simeq 0.01$ when a free nucleon is embedded in an iron nucleus. This is only a 20% ef-

fect, integrated over *all* x, but it may nevertheless be on the verge of a disagreement with experiment.

The predicted ratio $R_{\rm EMC}(x)=F_2^A(x)/F_2^N(x)$ takes on a particularly simple form at *exactly* $x=0$. From Eqs. (1.1), (3.3), and (3.5), we deduce

$$R_{\rm EMC}(0)\equiv\frac{F_2^A(0)}{F_2^N(0)}=1+\langle n_\pi\rangle\frac{F_2^\pi(0)}{F_2^N(0)}\ . \tag{3.15}$$

Correspondingly, if a straight-line fit to the EMC data in Fig. 1 is extended naively to $x=0$, we would deduce an immediate bound on $\langle n_\pi\rangle$, as long as $F_2^\pi(0)/F_2^N(0)$ is assumed to be known. As pointed out in Ref. 6, however, there are substantial difficulties associated with a straightforward application of Eq. (3.15).

In Sec. III A we discuss the nucleon and pion momentum densities in a nucleus, and in Sec. III B we describe our nucleon and pion parton densities. Readers not concerned with such questions may wish to proceed to Sec. IV in which results and comparisons with data are presented.

A. Nucleon and pion momentum distributions in a nucleus

Momentum densities $\rho_\pi(\mathbf{k})$ and $\rho_N(\mathbf{q})$ of mesons and nucleons in a nucleus can be obtained[16–18] from conventional nuclear theory as functions of the three-vector momenta $\mathbf{k}$ and $\mathbf{q}$. In Ref. 6, we showed how expressions for the light-front densities $f_\pi(y)$ and $f_N(z)$ needed in Eq. (1.1) can be obtained by relating these to $\rho_\pi(\mathbf{k})$ and $\rho_N(\mathbf{q})$.

With the definitions and approximations described in Secs. III and IV of Ref. 6 we have

$$f_N(z)=\int d^3q\,\rho_N(\mathbf{q})\delta\left[z-\frac{A[\mathbf{n}\cdot\mathbf{q}+(\mathbf{q}^2+m_N^2)^{1/2}]}{\langle\,|P|\,\rangle}\right] \tag{3.16}$$

and

$$f_\pi(y)=\int d^3k\,\rho_\pi(\mathbf{k})\times\delta(y-A[\mathbf{n}\cdot\mathbf{k}+(\mathbf{k}^2+m_\pi^2)^{1/2}]/\langle\,|P|\,\rangle)\ . \tag{3.17}$$

The number $\langle\,|P|\,\rangle$ is determined by the requirement (1.3). For $\rho_N(\mathbf{q})$ we use the Fermi-gas distribution smeared with an empirical radial density function $\rho(r)$ (Ref. 19). If $\langle N_B\rangle$ is the mean number of other baryons (other than nucleons) of baryon number n_B we have

$$\rho_N(\mathbf{q})=[(1-n_B\langle N_B\rangle)/A]\int d^3r\,\rho_F(\mathbf{q},r)\rho(r)\ , \tag{3.18}$$

where $\rho_F(\mathbf{q},r)$ is the Fermi-gas distribution for the density at distance r from the center. For deuterium the approximation $|P|\to\langle\,|P|\,\rangle$ is not valid. In that case we use the exact transformation

$$f_D(z)=\int d^3q\sum_L|u_L(q)|^2\delta(z-[\mathbf{n}\cdot\mathbf{q}+(\mathbf{q}^2+m_N^2)^{1/2}]/(\mathbf{q}^2+m_N^2)^{1/2})\ , \tag{3.19}$$

where the $u_L(q)$ are momentum-space partial-wave deuteron wave functions. The nucleon momentum distributions $f_N(z)$ for deuterium, aluminum, iron, and gold are shown in Fig. 3.

Since we identify $F_2^N(x)$ with the measured structure function of an isolated nucleon, including the effects of its pion cloud, the density $\rho_\pi(\mathbf{k})$ is the excess density due to pion exchange. As shown in Ref. 6, our formula for the momentum distribution of exchange pions is[16,17]

$$\rho_\pi(\mathbf{k})=-\langle\,|\omega_\pi^{-1}V_{\rm OPE}(\mathbf{k})|\,\rangle\frac{1}{A}\ . \tag{3.20}$$

For consistency it is essential that the one-pion-exchange (OPE) potential appearing explicitly in Eq. (3.20) be the same as that used in determining the many-body wave function used in calculating the expectation value. In particular, it makes no sense to change the size of the nucleon implied by the vertex function $|(\Lambda^2-m_\pi^2)/(\Lambda^2+\mathbf{k}^2)|^2$ without refitting the potential to the two-nucleon data. The value of Λ, $\Lambda=7$ fm^{-1} used in Ref. 16 corresponds to a small nucleon core size typical of nuclear potential models, but considerably smaller than that usually assumed in cloudy bag models. In order to include in a convenient manner at least a substantial fraction of the two-pion exchange effects we include Δ isobar states of the nucleons and use a Hamiltonian which includes $N\Delta\pi$ and $\Delta\Delta\pi$ vertices.[18] Two potentials V_{28} and V_{28Q} differ from each other in the strength of the $N\Delta\pi$ vertex: The "Chew-Low value" $(f_{N\Delta\pi}/f_{NN\pi})=2$ and the quark-model value $(f_{N\Delta\pi}/f_{NN\pi})=\sqrt{72/25}$ were used, respectively, in the construction of V_{28} and V_{28Q}. Both potentials give equally good fits to the two-body data. The momentum densities $\rho_\pi(\mathbf{k})$ were obtained in the manner described in

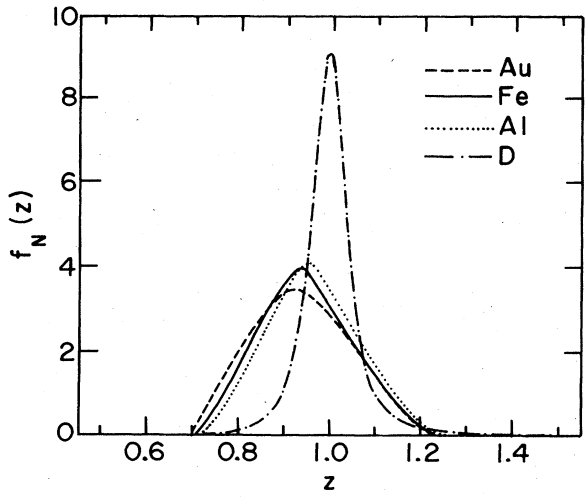

FIG. 3. The light-front momentum fraction distributions $f_N(z)$ of the nucleons in deuterium, aluminum, iron, and gold.

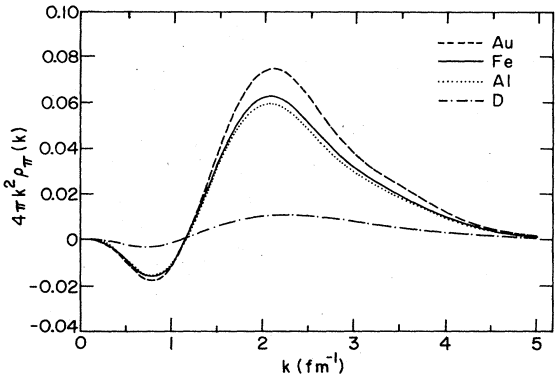

FIG. 4. The densities $4\pi k^2\rho_\pi(\mathbf{k})$ vs $\mathbf{k}$ for Au, Fe, Al, and D. These are normalized such that $\int d^3k\,\rho_\pi(\mathbf{k})=\langle n_\pi\rangle$.

Ref. 6 for deuterium and for homogeneous nuclear matter of different densities with both V_{28} and V_{28Q} (Ref. 18). The shape of the momentum distributions is virtually the same for both potentials, but the pion numbers $\langle n_\pi\rangle$ are smaller by a factor of about 0.73 for V_{28Q}. Clearly the value of $\langle n_\pi\rangle$ is to some extent model dependent. In the following we will use the results from V_{28Q} which yield good agreement with the SLAC data.

For aluminum, iron, and gold we have averaged nuclear-matter results over the appropriate nucleon densities.[19] The results obtained for the V_{28Q} nucleon-nucleon potential are shown in Fig. 4. The mean numbers of exchange pions per nucleon are $\langle n_\pi\rangle=0.02$, 0.09, 0.10, and 0.12 for D, Al, Fe, and Au, respectively. We note that $\langle n_\pi\rangle$ increases rapidly with A for small values of A, then tends to level off.[16] Qualitatively, this implies that both the slope of $R_{\rm EMC}(x)$ and its extrapolated intercept at $x=0$ should also increase rapidly for low values of A but then show little change with A for $A\gtrsim$ Al, in agreement with data.[2]

The corresponding light-front momentum distributions $f_\pi(y)$ for aluminum, iron, and gold are shown in Fig. 5. In Fig. 4 we note that the momentum distribution peaks near $k=3m_\pi$. Thus the "transverse mass," $(m_\pi^2+\mathbf{k}_T^2)^{1/2}$, which governs the gross shape of $f_\pi(y)$ cannot, even for qualitative purposes, be approximated by m_π. For small values of k the excess pion density $\rho_\pi(\mathbf{k})$ is negative due to Pauli blocking of the nucleon pion cloud. This feature shows up in $f_\pi(y)$ as a depression in the neighborhood of $y=0.2$. In the absence of this negative contribution $f_\pi(y)$ would be flat in the region between the two peaks. Our detailed investigations have shown, however, that the final results for $F_2^A(x,Q^2)$ are insensitive to the details of the functional shape of $f_\pi(y)$. The essential quantitative and qualitative features of our results for $R_{\rm EMC}(x)$ and $\bar q(x)$ are controlled by $\langle n_\pi\rangle$ and $\langle y\rangle$, defined in Eqs. (3.3) and (3.4).

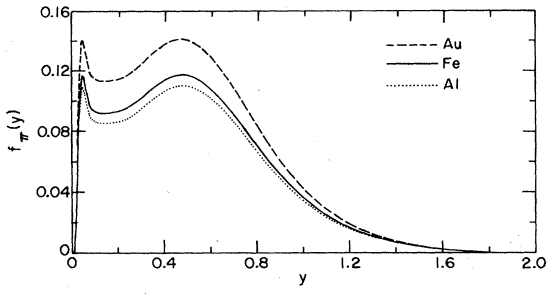

FIG. 5. The light-front momentum-fraction distribution $f_\pi(y)$ of exchange pions in aluminum, iron, and gold.

We note that our nucleon-nucleon potential includes $N\Delta\pi$ vertices. This means that in addition to pions we should explicitly treat Δ's as constituents of nuclei, using our Eq. (1.1) with $B\equiv\Delta$. However, the values computed[18] for $\langle n_\Delta\rangle$ are too small, ranging from $\langle n_\Delta^{\rm Al}\rangle=2.7\%$ to $\langle n_\Delta^{\rm Au}\rangle=3.4\%$, to alter F_2^A appreciably and we henceforth ignore them.

B. Pion and nucleon structure functions

In this section we specify the pion and nucleon structure functions $F_2^\pi(x,Q^2)$ and $F_2^N(x,Q^2)$ used throughout our analysis. For the nucleon's quark and antiquark densities we use the explicit parametrizations derived by the CERN-Dortmund-Heidelberg-Saclay (CDHS) collaboration[20] from fits to deep-inelastic νH_2 and $\bar\nu H_2$ data. In Fig. 6, we compare our computed free proton-quark densities with CDHS data which were extrapolated to $Q^2=15$ GeV^2 by the experimenters.[4] These data on xu_v,

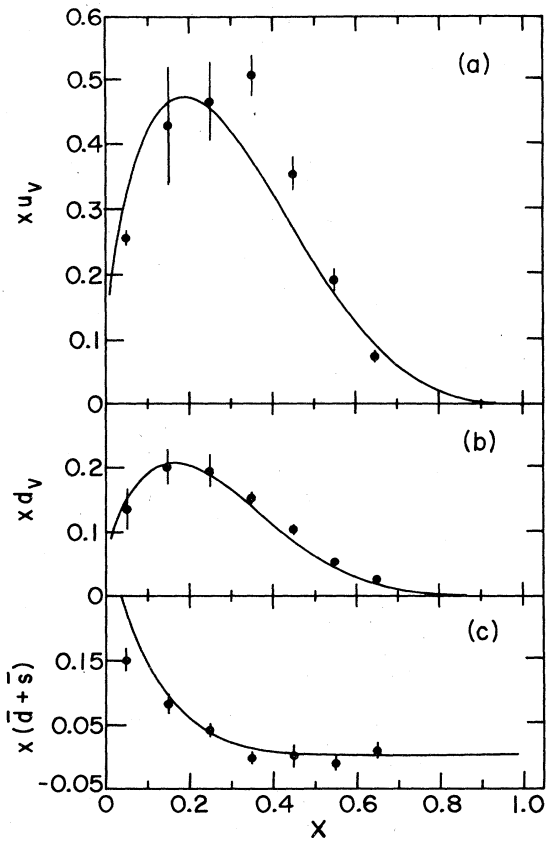

FIG. 6. Solid curves are computed from the CDHS parametrization (Ref. 20) which we employ. The data are from Ref. 4 at $Q^2=15$ GeV.^{2} In (a) we show the proton-valence-quark momentum distribution $xu_v(x)$; in (b) $xd_v(x)$; and in (c) the sea combination $x[\bar d(x)+\bar s(x)]$.

xd_v, and $x(\bar{d}+\bar{s})$ are consistent with analogous results extracted by the BEBC D_2 experiment.[21] The parametrizations we employ are in reasonable agreement with the (free nucleon) data in both shape and normalization. The same CDHS parametrizations are also in good agreement with CDHS and EMC data on $F_2^{\nu N}(x,Q^2)$ and $F_2^{\mu N}(x,Q^2)$.

Since the pion-quark densities, discussed below, are determined only near $Q^2 \simeq 25$ GeV^2, we choose for reasons of consistency to evaluate the CDHS nucleon-quark densities also at $Q^2=25$ GeV^2. Since no appreciable dependence on Q^2 is observed in the data set of any individual experiment, we believe our choice of $Q^2=25$ GeV^2 for our calculations does not bias our conclusions about $R_{\rm EMC}(x,Q^2)$ and $R_{\bar{q}}(x,Q^2)$. To discuss Q^2 dependence at fixed x more meaningfully, we would need a set of pion structure functions whose evolution with Q^2 is known to roughly the same precision as that of the CDHS nucleon structure functions. Even then, little residual dependence on Q^2 would be expected in the ratio, $R_{\rm EMC}=F_2^A(x,Q^2)/F_2^N(x,Q^2)$.

There are no measurements of deep-inelastic lepton scattering from pion targets, except possibly for the data discussed in this paper. However, if the Drell-Yan model is assumed to apply, structure functions may be extracted from data on massive lepton pair production $\pi N \to \gamma^* X$. A detailed analysis of this type was performed by the CERN NA10 collaboration,[22] resulting in a determination of the effective valence and ocean components of the pion-quark and antiquark densities for Q^2 in the neighborhood of 25 GeV^2. We shall use these NA10 functions in our analysis.

Because we are describing isoscalar nuclei, our pions are also "isoscalar" mesons containing equal numbers of up, down, anti-up, and anti-down quarks. Decomposing $q_f^{(\pi)}(x)$ into valence $V_\pi(x)$ and ocean $S_\pi(x)$ components, we write

$$u_\pi(x)=\bar{u}_\pi(x)=d_\pi(x)=\bar{d}_\pi(x)=\tfrac{1}{2}V_\pi(x)+S_\pi(x)\ , \tag{3.21}$$

$$s_\pi(x)=\bar{s}_\pi(x)=S_\pi(x)\ . \tag{3.22}$$

Since the number of valence quarks plus valence antiquarks in a pion is two, our normalization is

$$\int_0^1 V_\pi(x)dx=1\ . \tag{3.23}$$

We assume the ocean in the pion to be SU(3) symmetric. We obtain

$$F_2^{\mu\pi}(x)=x\left[\tfrac{5}{9}V_\pi(x)+\tfrac{4}{3}S_\pi(x)\right]\ . \tag{3.24}$$

The specific NA10 parametrization[22] of $V_\pi(x)$ which we use is

$$xV_\pi(x)=\frac{\Gamma(\alpha+\beta+1)}{\Gamma(\alpha)\Gamma(\beta+1)}x^\alpha(1-x)^\beta\ , \tag{3.25}$$

with $\alpha=0.36-0.074\bar{s}$ and $\beta=0.99+0.60\bar{s}$. Here

$$\bar{s}=\ln[\ln(Q^2/\Lambda^2)/\ln(Q_0{}^2/\Lambda^2)]\ ,$$

with $Q_0{}^2=25$ GeV^2 and $\Lambda=0.2$ GeV. For the ocean, we use

$$xS_\pi(x)=\frac{A_s}{6}(p+1)(1-x)^p\ , \tag{3.26}$$

with $p=8.7$, and $A_s=0.51-2\alpha/(\alpha+\beta+1)$. Together the valence and sea quarks carry 51% of the pion's momentum at $Q^2=25$ GeV^2; the ocean alone carries 20%.

IV. RESULTS AND COMPARISON WITH DATA

A. Pion-exchange model

In Fig. 7, for $\mu N \to \mu' X$, we present our calculated values of $R_{\rm EMC}(x,Q^2)$ as a function of x for three nuclei Al, Fe, and Au, and we compare these with available data. For all three nuclei, agreement between theory and experiment is acceptable for $x \gtrsim 0.3$. The rapid increase of $R_{\rm EMC}(x)$ as $x \to 1$ is due to Fermi smearing. In the region $x>0.6$, calculated values of $R_{\rm EMC}(x)$ are sensitive to features of the nuclear wave function which we have approximated in only a rough manner.

In Fig. 7(b), we note that agreement with the SLAC data extends down to $x \simeq 0.1$, but, below that value, effects in the data such as shadowing[23] begin to depress $R_{\rm EMC}(x)$ below unity. Such effects are not included in our model. For $x \lesssim 0.3$, the EMC data rise as $x \to 0$ substantially faster than our pion model can accommodate. On the other hand, if the normalization of the EMC data is reduced by 5%, then our theoretical curve is in excellent agreement, as shown in Fig. 7(c). This reduction is within the 7% normalization uncertainty quoted in Ref. 1.

The comparison with data in Fig. 7 indicates that we reproduce the weak A dependence of $F_2^A(x,Q^2)$ observed in the SLAC data. This dependence on A is illustrated more clearly in Fig. 8.

In Fig. 9, we present our expectations for the enhancement of the ocean, $R_{\bar{q}}(x)$, where

$$x\bar{q}(x)=x[\bar{u}(x)+\bar{d}(x)+2s(x)]\ .$$

We show results calculated with the V_{28Q} and V_{28} nucleon-nucleon potentials, as well as the effects of an arbitrary additional enhancement of the nucleon ocean by 10% to 15%. For $x \lesssim 0.3$, the V_{28} and V_{28Q} potentials lead to an $R_{\bar{q}}(x)$ well within the range of values quoted by the CDHS collaboration[4] [cf. Eq. (2.15)] $K_{\bar{q}}=1.10 \pm 0.11(\text{stat}) \pm 0.07(\text{syst})$, and consistent with the bounds obtained from bubble-chamber results.[5] For V_{28}, we compute $K_{\bar{q}}=1.14$, and for V_{28Q}, $K_{\bar{q}}=1.11$. For an arbitrary additional enhancement of the nucleon ocean by 10% or 15% $K_{\bar{q}}$ rises to 1.20 or 1.25, respectively. An enhancement of 15% is at best marginally within the experimental limits. [Our computed values of $K_{\bar{q}}$ are obtained upon integrating numerator and denominator of $R_{\bar{q}}(x)$ from $x=0.01$ to $x=0.5$.] The increase of $R_{\bar{q}}(x)$ predicted by our model as x increases beyond $x \approx 0.3$ is associated with valence antiquarks in the exchange pions. It occurs in a kinematic region in which the ocean itself observed to be negligibly small experimentally.

Especially in view of the possibility that the magnitude of the rise in $R_{\rm EMC}(x,Q^2)$ at small x may not be confirmed by future experiments, we note that all other

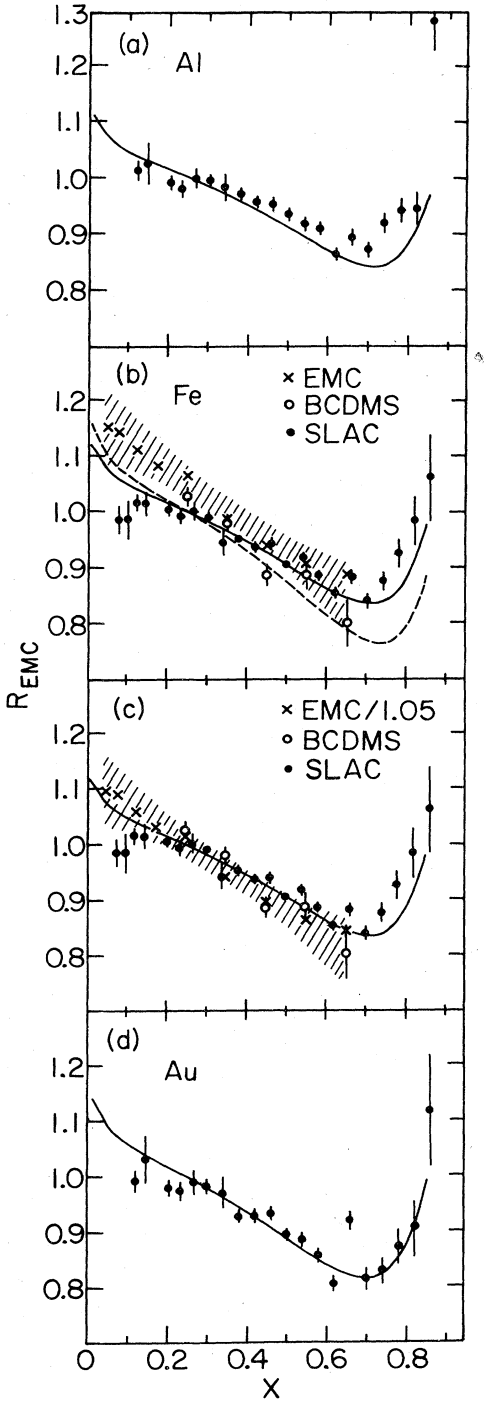

FIG. 7. Computed values of $R_{EMC}(x,Q^2)$ versus x for $\mu N \to \mu' X$, for three nuclei; (a) Al, (b) and (c) Fe, and (d) Au. In all cases, we use CDHS structure functions at $Q^2=25$ GeV^2. For the solid curves we use the function $f_\pi(y)$ evaluated from the V_{28Q} potential which provides (a) $(\langle n_\pi\rangle, \langle y\rangle)=$ (0.089, 0.049); (b) and (c) $(\langle n_\pi\rangle,\langle y\rangle)=$ (0.095, 0.052); (d) $(\langle n_\pi\rangle,\langle y\rangle)=$ (0.114, 0.061). The dashed curve in (b) is from the V_{28} potential for which $\langle n_\pi\rangle=0.13$ and $\langle y\rangle=0.067$. Except for (c), the data are those from Refs. 1–3. In (b), we show the EMC data, Ref. 1, divided by 1.05.

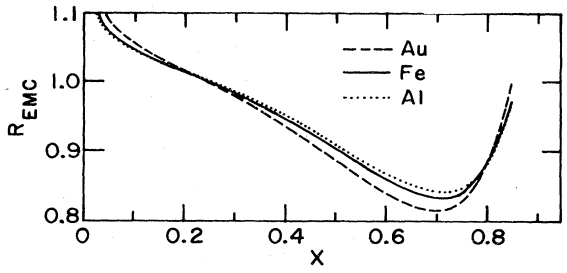

FIG. 8. Theoretical curves shown in Fig. 7 are superimposed in order to exhibit the A dependence of the effect.

features of the present data on R_{EMC} and $R_{\bar{q}}$ are in excellent agreement with our approach based on conventional nuclear theory.

One might consider increasing $\langle n_\pi\rangle$ and modifying $\langle y\rangle$ in an attempt to devise a function $R_{EMC}(x)$ which comes closer to reproducing the unadjusted EMC data points for $x<0.3$ in Fig. 7(b). However, as we discussed in some detail in Ref. 6, a large enough increase in $\langle n_\pi\rangle$ to accommodate the EMC data at small x inevitably causes an unacceptably deep depression in $R_{EMC}(x)$ at intermediate x values, in the neighborhood of $x\simeq 0.5$. Since all three data sets in Fig. 7(b) appear to agree on the magnitude of $R_{EMC}(x)$ in the intermediate x range, we cannot

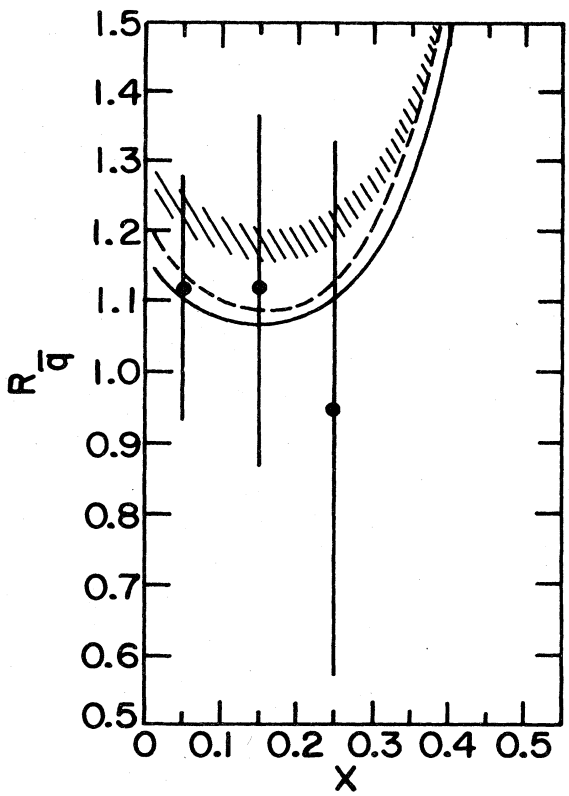

FIG. 9. Theoretical antiquark enhancement $R_{\bar{q}}(x)$ compared with the data of Ref. 4. The solid and dashed curves are calculated with the V_{28Q} and V_{28} models, respectively. The shaded band shows the effect of an additional 10% to 15% enhancement of the nucleon's ocean.

motivate the necessary increases in $\langle n_\pi \rangle$, even on purely phenomenological grounds. We note, however, that the necessary large increase ($\langle n_\pi \rangle \gtrsim 0.3$) would be unacceptable because of its implications for $K_{\bar{q}}$, and inconsistent with the nuclear models upon which our work is based.

To achieve agreement with the unadjusted EMC data for all x we must abandon the assumption that the nucleon structure function is left affected by the medium. Only modest modifications are needed. For example, to account for medium-dependent effects, we considered the following simple representations of the valence an sea-quark distributions of nucleons in an iron nucleus. In the medium, we make the replacements

$$xV^N(x) \to (1-D)xV^N(x) + DxV'_N(x) , \tag{4.1}$$

$$xS^N(x) \to (1+D_s)xS^N(x) , \tag{4.2a}$$

and

$$xs^N(x) \to (1+D_s)xs^N(x) . \tag{4.2b}$$

On the right-hand side of Eqs. (4.1) and (4.2), functions $V^N(x)$, $S^N(x)$, and $s^N(x)$ are the free nucleon structure functions defined in Eqs. (2.6)—(2.8) and computed from the CDHS functions discussed in Sec. III C. In Eqs. (4.1) and (4.2), D and D_s are adjustable constants. We parametrize $V'_N(x)$ as

$$xV'_N(x) = d_N x^Q (1-x)^P (1+cx^R) \tag{4.3}$$

with d_N chosen to maintain the valence-quark normalization condition $\int_0^1 V'_N(x)dx = \frac{3}{2}$; Q, P, and R are adjustable constants.

Using the new functions $V^N(x)$, $S^N(x)$, and $s^N(x)$ in our convolution formulas, we find that many different choices of the parameters (D, D_s, Q, P, R) serve to produce acceptable fits to the EMC data. As an illustration, a 10% enhancement of the nucleon ocean with no change in the valence structure fits on the BCDMS data and is consistent with the small-x EMC data within the stated errors [Fig. 10(a)]. A modest change in the valence structure (Fig. 11) with no enhancement of the ocean produces a curve consistent with the EMC data for all x [Fig. 10(b)].

The additional ocean represented in Eq. (4.2) by a value $D_s > 0$ may arise from an enhancement of the pion cloud of individual nucleons, as discussed by Ericson and Thomas[7] and by Llewellyn Smith.[7] Using the "toy model" function of Ref. 6, $g_\pi(y)$ with $a=1$ and $b=3$, to imitate their $f_\pi(y)$, we computed the medium-dependent modification of the nucleon ocean as

$$\bar{q}^A(x) = \bar{q}^N(x) + \int_{y \geq x} \frac{dy}{y} g_\pi(y) \bar{q}^\pi \left(\frac{x}{y} \right) ,$$

with $\int g_\pi(y)dy = c_\pi$. We find that the antiquark distribution computed this way has essentially the same x dependence as the antiquark distribution of the nucleon according to the CDHS parametrization. Computing an enhancement of the nucleon ocean in this manner, and taking $c_\pi = 0.12$, we obtain the results shown in Fig. 10(c). The agreement with $R_{\rm EMC}(x)$ is certainly acceptable. However, we emphasize that to obtain this agreement we require an enhancement of the ocean of individual nucleons as well as the effects of the exchange pions in the nucleus.

As remarked in Sec. II, the SLAC data on $R_{\rm EMC}(x)$ may be brought into agreement with the original EMC data if one assumes that σ_L/σ_T grows with A. We have

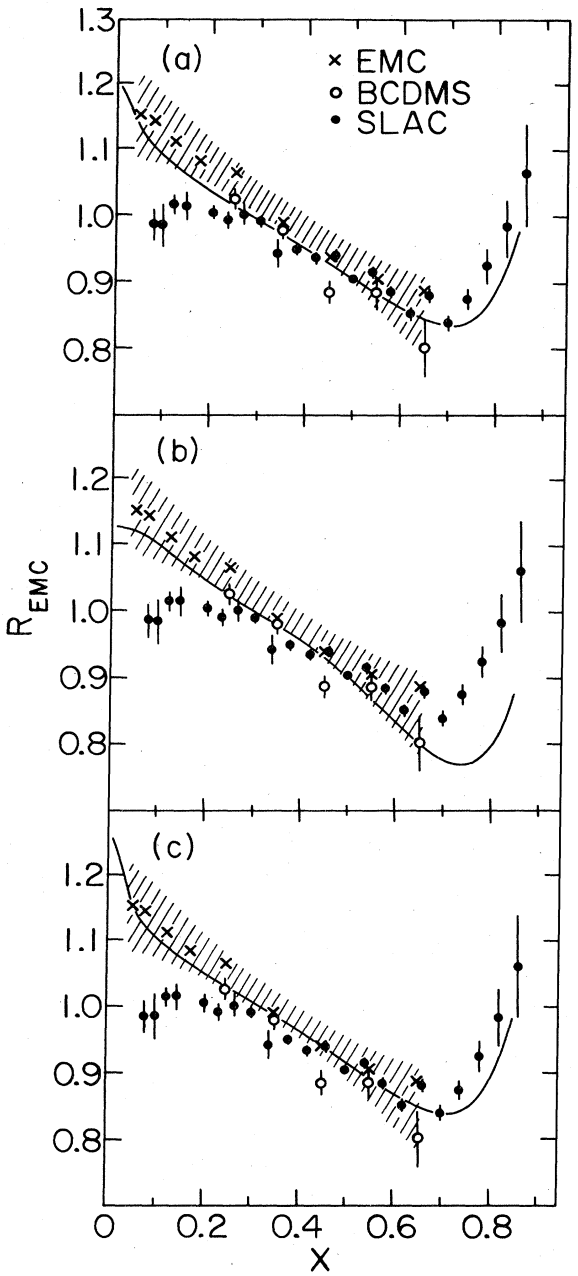

FIG. 10. The ratio $R_{\rm EMC}(x)$ of the structure functions obtained from the pion exchange model with an additional *ad hoc* alteration of the nucleon's quark structure. (a) Multiplicative enhancement of the ocean, no change in the valence distribution; $D=0$, $D_s=0.1$. (b) No change in the ocean. Change of valence-quark distribution shown in Fig. 11. (c) No change in the valence distribution. The additional ocean enhancement was calculated assuming an increase in the nucleon's pion cloud as described in the text; $c_\pi = 0.12$.

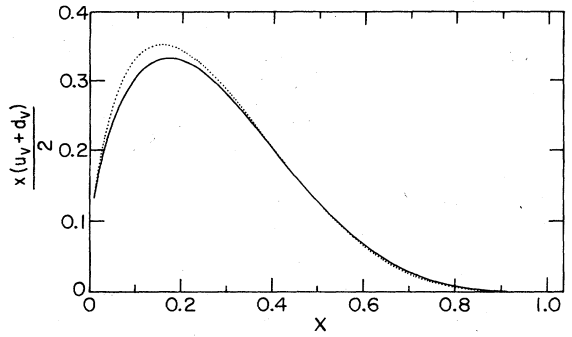

FIG. 11. Change in the nucleon's valence-quark distribution used in Fig. 10(b). The solid curve is the unmodified CDHS parametrization. The dotted curve is calculated from Eqs. (4.1) and (4.3) with the parameters $D=0.2$, $Q=0.7$, $P=6$, $R=3$, $c=18$.

considered whether such dependence on A can be expected from our model, especially since scattering from an integer spin target can produce large values of σ_L/σ_T near kinematic limits.[24] Unfortunately, because the effects of the exchange pions on $F_1(x,Q^2)$ and $F_2(x,Q^2)$ are themselves so small, particularly at small x, we do not predict any substantial growth of σ_L/σ_T with A.

B. Rescaling and possible change in confinement scale

In a recent series of papers[9] it has been argued that the EMC effect may be explained in terms of a change in the effective value of Q^2 in nuclei. Specifically, a "rescaling parameter" $\xi_A(Q^2)$ is introduced, and it is postulated[9] that

$$F_2^A(x,Q^2)=F_2^N(x,\xi_A(Q^2)Q^2)\ . \tag{4.4}$$

For $Q^2=20$ GeV^2, the value $\xi_{\rm Fe}=2.02$ is claimed[9] to provide good agreement with the EMC data.[1] We test this hypothesis using the CDHS structure functions[20] employed throughout this paper. In Fig. 12 we compare results obtained from Eq. (4.4) with data and with the results of our model. Following Ref. 9 we assume $Q^2=(200x+10)$ GeV^2 and

$$\xi(Q^2)=\xi(Q_0^2)^{[\alpha_s(Q_0^2)/\alpha_s(Q^2)]}\ . \tag{4.5}$$

The rescaling model yields a ratio $R_{\rm EMC}(x)$ which agrees qualitatively with the trend of the data, but it does less well than our conventional nuclear model. To bring the rescaling model into accord with the data one would have to assume an error of 7.5% in the relative normalization of the iron and deuterium data,[25] which is at the outside edge of the possible uncertainty quoted in Ref. 1. To examine whether the poor agreement in Fig. 12(a) might be due to our choice of structure functions, we computed the ratio $F_2^{\rm Fe}(x,Q^2)/F_2^{\rm Fe}(x,Q^2/\xi)$ using published[26] EMC data for $F_2^{\rm Fe}(x,Q^2)$. The points so obtained are in agreement with the Q^2 rescaling curve shown in Fig. 12(a). We also repeated our computations using the Duke-Owens structure functions.[27] We obtained essentially identical results.

The similarity of the trends of the EMC data and the rescaling curve has led to broad acceptance[28] of the qualitative conclusion that the quark confinement scale increases when a free nucleon is embedded in a nucleus. While this concept may be correct physically, we find little quantitative support for it from the curve shown in Fig. 12(a).

V. CONCLUSIONS AND DISCUSSION

In this paper we have examined in detail a model based on the conventional picture in which nucleons and pions are the relevant hadrons in nuclei. In this model, differences between the free nucleon and nuclear structure functions are due to scattering from exchange pions in nuclei.

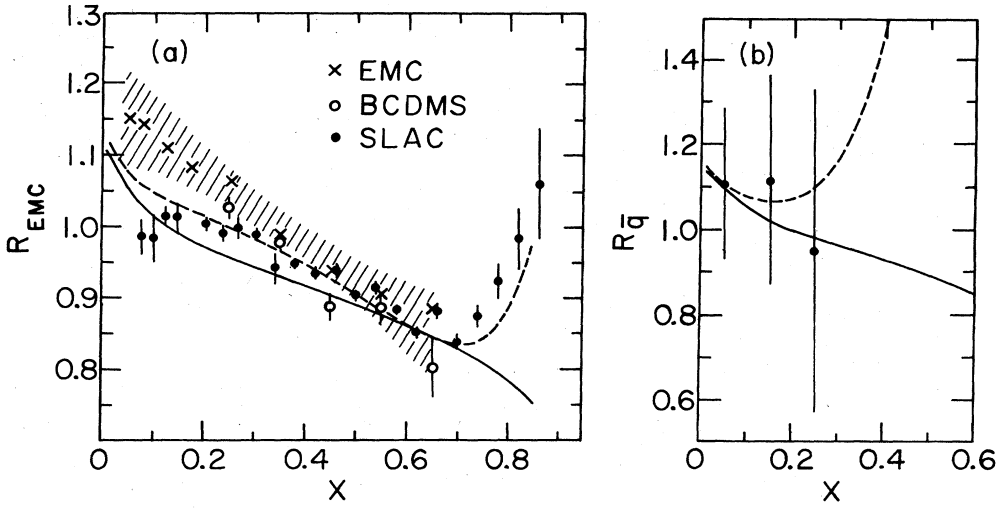

FIG. 12. Comparison of the rescaling prescription with data and with our model. The solid curve shows Q^2 rescaling with $Q^2=(200x+10)$ GeV^2 and ξ_A given by Eq. (4.5). The dashed curve shows our results. (a) $R_{\rm EMC}$, (b) $R_{\bar{q}}$.

The three main ingredients of our approach are these: We assume that nuclei are bound systems of nucleons and mesons. Second, we assume that the quark and antiquark momentum distributions, and thus, the deep-inelastic structure functions of these nucleons and mesons are unaffected by the nuclear medium. Third, we retain the usual assumption that nucleons contribute incoherently to the structure function of the nucleus, and we add the same incoherence assumption for the pions. We obtain the nuclear structure functions as a sum of convolutions of (measured) isolated-hadron structure functions with hadron momentum distributions derived from nuclear Fock-space wave functions. The nucleon and pion momentum distributions in a nucleus are derived from nuclear potential models. Based on the results reported here, we have developed the following point of view regarding the A-dependent effects observed experimentally in $F_2^A(x,Q^2)$ and $\bar{q}^A(x,Q^2)$.

(i) The antiquark density is increased modestly at small x, by about 10% in our conventional nuclear model, entirely consistent with all data sets.

(ii) In our model, a modest increase is expected in $R_{\rm EMC}(x,Q^2)$ at small x ($x \lesssim 0.2$). In the SLAC data at low Q^2, this increase may be offset partially by shadowing effects. The increase we compute is too small to account for the magnitude of the original EMC results, but our model reproduces all data if we reduce the experimental $R_{\rm EMC}(x,Q^2)$ by 5%, which is within the 7% normalization uncertainty quoted in Ref. 1. The unmodified EMC data may indicate the presence of additional physics, whose importance may grow with Q^2, and which is outside the scope of our model.

(iii) The magnitude of the depression of $R_{\rm EMC}(x,Q^2)$ below unity for $0.3<x<0.8$ is reproduced well by our model, as is its dependence on A. There are two origins to the effect, both associated with momentum conservation. Because of Fermi smearing of the nucleon's quark distribution, $R_{\rm EMC}(x,Q^2)$ is depressed below unity for $x \lesssim 0.8$, and the momentum taken away by the exchange pions depresses it further.

(iv) The rise of $R_{\rm EMC}(x,Q^2)$ at $x \to 1$ is associated with Fermi smearing.

(v) Our model does not lead us to expect any significant growth of σ_L/σ_T with A. If such an effect is confirmed in further more precise experimental work now in progress, it would require an explanation outside the scope of our model. From the point of view of our model, we would be surprised if the A dependence of σ_L/σ_T is confirmed as an explanation for the differences between the EMC and SLAC data on $R_{\rm EMC}(x,Q^2)$ at small x.

(vi) We expect little dependence on Q^2 in $R_{\rm EMC}(x,Q^2)$ and $R_{\bar{q}}(x,Q^2)$ and essentially none is observed within the range of values of Q^2 studied in the individual experiments.

(vii) Rescaling models[9] do not provide a quantitative explanation $R_{\rm EMC}(x,Q^2)$, unless the EMC data are reduced in normalization by 7.5%, as assumed in Ref. 9.

All features of the data but one are reproduced by the conventional nuclear model which we study. The exception is the magnitude of the excess above unity of the ratio $R_{\rm EMC}(x)=F_2^A(x)/F_2^{\rm D}(x)$ for $x<0.2$, observed only by the original EMC experiment,[1] but even this can be accounted for if we reduce the normalization of the EMC data by 5%. If the magnitude of the low-x enhancement in $R_{\rm EMC}$ is confirmed, its explanation requires a modification of one or more of the three basic assumptions stated above. In a picture in which a free nucleon is represented as a core surrounded by a cloud of mesons, it seems plausible that the properties of the cloud would be modified when the nucleon is embedded in a nucleus. This would imply that the nucleon structure function itself $F_2^N(x,Q^2)$ is altered, in contrast to one of our assumptions. We find that we can reproduce the magnitude of the low-x enhancement of the EMC ratio, without violating any other data, if, in addition to the effects of the exchange pions, we introduce an *ad hoc* increase of the nucleon ocean in iron by about 10%. This increase could be interpreted as an increase of the pion cloud of individual nucleons. On the other hand, the same effect could also be achieved by a modest alteration of the valence structure without an *ad hoc* increase of the ocean. Such an alteration of the valence-quark distribution could not easily be blamed on the pion cloud and may be indicative of a large core size, or the presence of other baryon states in the nucleus. Because the low-x enhancement in $R_{\rm EMC}(x,Q^2)$ is observed only for $Q^2 \gtrsim 10$ GeV^2, it is possible that there is a threshold in Q^2 associated with the A-dependent alteration of $F_2^N(x,Q^2)$. From the point of view of demonstrating clearly that the nuclear medium affects the parton degrees of freedom, it is essential to carry out a careful series of experiments focused on the Q^2 and A dependences of $F_2^A(x,Q^2)$ at small x ($0<x<0.2$). Precise neutrino data on $R_{\bar{q}}(x)$ seem absolutely crucial for delineating whether the rise in $R_{\rm EMC}(x)$ at small x is associated principally with a modification of the valence or ocean distribution. In this context, we recall our remark in Sec. III that our pion model yields essentially no modification of the valence-quark distributions at small x [cf. Eq. (3.9)].

ACKNOWLEDGMENTS

We are indebted to R. Wiringa for the computations of $\rho_\pi(\mathbf{k})$ and discussions. This work was performed under the auspices of the United States Department of Energy under Contract No. W-31-109-ENG-38.

[1]European Muon Collaboration, J. J. Aubert, *et al.*, Phys. Lett. **123B**, 275 (1983).

[2]A. Bodek *et al.*, Phys. Rev. Lett. **50**, 1431 (1983); **51**, 534 (1983); R. G. Arnold *et al.*, Phys. Rev. Lett. **52**, 727 (1984).

[3]Bologna-CERN-Dubna-Munich-Saclay (BCDMS) collaboration (CERN Experiment NA4), as quoted by I. A. Savin, Rapporteur report at the *International Conference on High Energy Physics,* Leipzig, 1984, edited by A. Meyer and E.

Wieczorek (Academie der Wissenschaften der DDR, Zeuthen, DDR, 1984).

[4]CERN-Dortmund-Heidelberg-Saclay (CDHS) collaboration, H. Abramowicz *et al.*, Z. Phys. C **25**, 29 (1984).

[5]BEBC TST collaboration, M. A. Parker *et al.*, Nucl. Phys. **B232**, 1 (1984); BEBC D_2 (WA25) and Ne (WA59) collaborations, A. M. Cooper *et al.*, Phys. Lett. **141B**, 133 (1984); A. M. Sarkar-Cooper, CERN Report No. CERN/EP 84-121, 1984 (unpublished).

[6]E. L. Berger, F. Coester, and R. B. Wiringa, Phys. Rev. D **29**, 398 (1984).

[7]C. H. Llewellyn Smith, Phys. Lett. **128B**, 107 (1983); M. Ericson and A. W. Thomas, *ibid.* **128B**, 112 (1983); C. H. Llewellyn Smith, in *Particles and Nuclei,* proceedings of the Tenth International Conference, Heidelberg, 1984, edited by B. Povh and G. zu Pulitz [Nucl. Phys. **A434**, 35c (1985)]; A. W. Thomas, Phys. Lett. **126B**, 97 (1983); D. Stump *et al.*, in *Hadron Substructure in Nuclear Physics,* proceedings of the Conference, Indiana University, 1983, edited by W-Y. P. Hwang and M. H. MacFarlane (AIP, New York, 1984), p. 339.

[8]R. L. Jaffe, Phys. Rev. Lett. **50**, 228 (1983); Phys. Rev. D **11**, 1953 (1975); Comments Nucl. Part. Phys. **13**, 39 (1984).

[9]F. E. Close *et al.*, Phys. Lett. **129B**, 346 (1983); R. L. Jaffe *et al.*, *ibid.* **134B**, 449 (1984); F. E. Close *et al.*, Phys. Rev. D **31**, 1004 (1985); J. Cleymans and R. Thews, *ibid.* **31**, 1014 (1985).

[10]H. J. Pirner and J. P. Vary, Phys. Rev. Lett. **46**, 1376 (1981); C. E. Carlson and T. J. Havens, *ibid.* **51**, 261 (1983); M. Chemtob and R. Peshanski, J. Phys. G **10**, 599 (1984); B. C. Clark *et al.*, Phys. Rev. D **31**, 617 (1985).

[11]J. Dias de Deus *et al.*, Phys. Rev. D **30**, 697 (1984); G. B. West, Los Alamos Reports Nos. LA-UR-83-2504 and LA-UR-84-241 (unpublished); and in *Intersections Between Particle and Nuclear Physics,* proceedings of the conference, Steamboat Springs, 1984, edited by R. E. Mischke (AIP, New York, 1984), p. 360; J. P. Vary, in *Hadron Substructure in Nuclear Physics* (Ref. 7), p. 171; T. A. Carey *et al.*, Phys. Rev. Lett. **53**, 144 (1984); H. Esbensen, H. Toki, and G. F. Bertsch, Phys. Rev. C **31**, 1816 (1985); O. Nachtman and H. J. Pirner, Z. Phys. C **21**, 277 (1983); S. Date and A. Nakamura, Prog. Theor. Phys. **69**, 565 (1983); H. Faissner and B. R. Kim, Phys. Lett. **130B**, 321 (1983); N. N. Nikolaev, Usp. Fiz. Nauk **134**, 369 (1981) [Sov. Phys. Usp. **24**, 531 (1981)]; W. Furmanski and A. Krzywicki, Z. Phys. C **22**, 391 (1984); J. Szwed, Phys. Lett. **128B**, 245 (1983); G. Berlad, A. Dar, and G. Eilam, Phys. Rev. D **22**, 1547 (1980); G. Baym, Physica **96A**, 131 (1979); A. Krzywicki, Phys. Rev. D **14**, 152 (1976); L. L. Frankfurt and M. I. Strickman, Phys. Rep. **76**, 215 (1981); Nucl. Phys. **B181**, 22 (1981); M. Chemtob, *ibid.* **A336**, 299 (1980).

[12]Y. Sacquin, in *New Particle Production,* proceedings of the XIX Rencontre de Moriond, edited by J. Tran Thanh Van (Editions Frontières, France, 1984), Vol. 2, p. 659; I. A. Savin and G. Smirnov, Phys. Lett. **145B**, 438 (1984).

[13]E. L. Berger, in *Proceedings of the Workshop on Drell-Yan Processes,* Fermilab, 1982, edited by E. L. Berger, P. Malhotra, R. Orava, and H. Thacker (Fermilab, Batavia, Illinois, 1982), pp. 1—62 (see Sec. II E); Y. Gabellini in *New Particle Production* (Ref. 12), p. 645; R. Bickerstaff, M. Birse, and G. Miller, Phys. Rev. Lett. **53**, 2532 (1984); M. Ericson and A. Thomas, Phys. Lett. **148B**, 191 (1984).

[14]A. S. Ito *et al.*, Phys. Rev. D **23**, 604 (1981).

[15]P. A. M. Dirac, Rev. Mod. Phys. **21**, 392 (1949).

[16]B. L. Friman, V. R. Pandharipande, and R. B. Wiringa, Phys. Rev. Lett. **51**, 763 (1983); see Eq. (6).

[17]F. Coester, in *Recent Progress in Many Body Theories,* proceedings of the Third International Conference, Odenthal-Altenberg, Germany (Lecture Notes in Physics, Vol. 198), edited by H. Kümmel and M. L. Ristig (Springer, Berlin, 1984), p. 16.

[18]R. B. Wiringa, R. A. Smith, and T. L. Ainsworth, Phys. Rev. C **29**, 1207 (1984); R. B. Wiringa, in *Recent Progress in Many Body Theories* (Ref. 17), p. 44; and (private communication).

[19]At. Data Nucl. Data Tables **14**, 479 (1974).

[20]CERN-Dortmund-Heidelberg-Saclay collaboration, F. Eisele, in *Proceedings of the 21st International Conference on High Energy Physics, Paris, 1981,* edited by P. Petiau and M. Porneuf [J. Phys. (Paris) Colloq. **43**, C3-337 (1982)], and (private communications).

[21]D. Allasia *et al.*, Phys. Lett. **135B**, 231 (1984).

[22]CERN—Naples—Ecole Polytechnique—Strasbourg—Eidgen össiche Technishe Hochschule collaboration (CERN NA10), B. Betev *et al.*, CERN Reports Nos. CERN-EP/85-03 and CERN-EP/85-04, 1985 (unpublished).

[23]G. Gramer and J. Sullivan, in *Electromagnetic Interactions of Hadrons,* edited by A. Donnachie and G. Shaw (Plenum, New York, 1978), Vol. 2, p. 195. Important shadowing effects ($R_{EMC} < 1$) may be expected at very small x; see, e.g., A. Mueller, in *Proceedings of the XVIIth Rencontre de Moriond, Les Arcs, France, 1982,* edited by J. Tran Thanh Van (Editions Frontières, Gif-sur-Yvette, 1982), Vol. 1, and references therein.

[24]E. L. Berger and S. J. Brodsky, Phys. Rev. Lett. **42**, 940 (1979); L. Abbott, E. L. Berger, R. Blankenbecler, and G. Kane, Phys. Lett. **88B**, 157 (1979).

[25]This assumption is made in Ref. 9.

[26]J. J. Aubert, Phys. Lett. **105B**, 332 (1981).

[27]D. Duke and J. Owens, Phys. Rev. D **30**, 49 (1984); **30**, 49(E) (1984).

[28]J. V. Noble, Phys. Rev. Lett. **46**, 412 (1981); M. Jändel and G. Peters, Phys. Rev. D **30**, 1117 (1984); L. S. Celenza, *et al.*, Phys. Rev. Lett. **53**, 892 (1984); T. Goldman and G. J. Stephenson, Jr., Phys. Lett. **146B**, 143 (1984); G. Chanfray, *et al.*, *ibid.* **147B**, 249 (1984); M. Rho, Phys. Rev. Lett. **54**, 767 (1985).